16TH EUROPEAN CONFERENCE ON EARTHQUAKE ENGINEERING THESSALONIKI 18 - 21 JUNE 2018

SPATIAL VARIBILITY OF CPT DATA FOR LIQUEFACTION ASSESSMENT

Rose Line SPACAGNA[1], Luca PAOLELLA[2], Alessandro RASULO[3], Giuseppe MODONI[4]

ABSTRACT

The seismic liquefaction is often responsible for the major part of the economic losses caused by earthquakes. Usually damages involve the foundations of buildings, bridges, embankments, underground constructions and are widely diffused over the cities. The strategies for the mitigation of risk aim to evaluate susceptibility and hazard on given areas by quantifying the liquefaction potential indexes from the results of fast investigations. The empirical relations proposed in the literature based on the results of cone penetration tests CPT, allow to calculate the indexes at each vertical, which can be reductive for the complete risk assessment of larger territorial extension. The present study moves at two distinct levels, one carried out with traditional geographic information systems aiming to map the liquefaction hazard over the territory, the second one aiming to define the three-dimensional distribution of the liquefiable deposit in the subsoil.
The analysis focuses on the district of San Carlo, in the municipality of Sant'Agostino (Italy), located near the epicenter of the 2012 Emilia Romagna earthquake (Mw = 6.15). Several dozens of CPT profiles have been processed to compute the liquefaction potential maps and the individuation of the liquefiable deposits, using geostatistical methodologies. The results, validated with the observations of ground failures and damaged buildings recorded after the earthquake and with the geological structure of the investigated area, improve the quality of Microzonation studies with the addition of the liquefaction hazard and helps to precisely identify the susceptible subsoil deposit.

Keywords: seismic hazard, liquefaction, spatial variability, geostatistical analysis.

1. INTRODUCTION

The experience from the last earthquakes (Tohoku, 2011; Kumamoto, 2016; Christchurch 2010, 2011 and 2016, Emilia Romagna, 2012), has revealed that liquefaction is often the major causes for the economic loss induced by earthquakes. For this reason, the quantification of the hazard connected with liquefaction and the prediction of its effects has become an important part of the seismic risk assessment and incorporated into national and international standards (e.g. CTMS, 2017). The assessment becomes compulsory for areas, e.g. lowland or reclaimed lands, where high probability of earthquake occurrence is associated to particularly susceptible geological conditions.
However, considering the very large extension of the potentially affected areas, the evaluation of liquefaction susceptibility is not simple, mostly because of a large quantity of investigations needed to detect the subsoil with sufficient accuracy and due to the difficulty to process always larger amounts of data. The most common nowadays adopted strategy estimates the liquefaction hazard by computing indicators of the liquefaction potential starting from the results of in-situ tests. Methods have been developed based on in situ tests, Standard Penetration, Cone Penetration, Dilatometer and Sonic test being the most popular. Among the most widely used, a class of methods associates the triggering of liquefaction at the different depths to the outcomes of cone penetration tests (CPT), exploiting the advantage of these tests to obtain continuous logs throughout the investigated depth with relative low

[1]University of Cassino and Southern Lazio, Cassino, Italy, rlspacagna@unicas.it
[2]University of Cassino and Southern Lazio, Cassino, Italy, luca.paolella@unicas.it
[3]University of Cassino and Southern Lazio, Cassino, Italy, a.rasulo@unicas.it
[4]University of Cassino and Southern Lazio, Cassino, Italy, modoni@unicas.it

effort. Liquefaction potential indexes are then computed at specific sites by integrating these effects over the whole depth.
Considering that liquefaction usually involves large portions of the subsoil, there is the need to assemble the results obtained on the different points into more general studies extended to the whole investigated area. This step entails the need for processing a considerable amount of data and for providing a spatial representation of the outcomes over the investigated territory.
Conventionally, the liquefaction potential is represented on maps that quantify the seismic hazard at a sufficiently large scale to interact with the management and planning of the territory (Microzonation). These maps can be conveniently used to assess the risk connected with liquefaction on structures and infrastructures present on the territory, to predict the related economic loss and the resilience of the urban system and its community, and to plan mitigation strategies.
In a strict sense, these studies can be carried out only on locations where data are available, i.e. where field tests have been performed. However, previous studies have demonstrated that it is possible to extend the assessment of liquefaction potential also on areas where in situ test are not availed (Liu and Chen, 2006; Pokhrel et al., 2013) by implementing of interpolation techniques. In spite of their undisputable advantage, it must be considered that the reliability of these studies may be very questionable if the errors of the made estimates are not properly taken into account.
The present study aims to contribute at increasing the reliability of the above studies, introducing different geostatistical methodologies (Chiles and Delfiner, 1999) for the spatial delimitation of the deposits susceptible of liquefaction. The analysis moves at two distinct levels, one carried out with traditional geographic information systems aiming to map the liquefaction hazard over the territory, the second one aiming defining the three-dimensional extension of the liquefiable deposit in the subsoil.
After a brief introduction of the adopted algorithms, the methodology is applied to a case study. The study is carried out for the district of San Carlo, in the municipality of Sant'Agostino (Italy), extensively affected by liquefaction during the 2012 Emilia Romagna earthquake (Mw = 6.15). Based on the available dataset of in situ tests, the work has been aimed at drawing maps of different indicators of the liquefaction potential, quantifying the reliability of the predictions with a geostatistical analysis.

2. LIQUEFACTION HAZARD

2.1 Liquefaction potential indicators

The liquefaction hazard at a single position of the territory is studied by quantifying indicators of the liquefaction potential on vertical profiles investigated with CPT tests. In particular, the triggering of the phenomenon is firstly evaluated at each investigated depth by computing the Liquefaction Safety Factor (Equation 1), given by the ratio between the Cyclic Resistance Ratio "CRR" and the Cyclic Stress Ratio "CSR".

$$FSL = \frac{CRR}{CSR} \tag{1}$$

The CSR is defined by ratio between the cyclic shear stress induced by the earthquake and the stress state in situ (Seed and Idriss, 1971). Numerous algorithms are proposed in the literature to compute CRR from the tip and frictional sleeve resistance of CPT test (Robertson and Wride, 1998; Idriss and Boulanger, 2008). In this work, the most recent method developed by Boulanger and Idriss (2014) has been adopted. According to this method, the liquefiable layers is the one where FSL is lower than one, provided that the index material I_c defined by Robertson and Cabal (2010) ranges between 1.31 and 2.6, i.e. is representative of sandy soils) and that the layer is saturated.
The FSL can be thus integrated in different forms to quantify the effects of liquefaction at the ground level. In this paper, the following three alternative methods are examined:

a) "Liquefaction Potential Index - LPI" (Iwasaki et al., 1978)

   The indicator is computed with the following integral function:

$$LPI = \int_{0\ m}^{20\ m} F_1(z) \cdot W(z) \cdot dz \quad (2)$$

where z is the depth, and W(z) is a weighting factor computed as follows:

$W(z) = 10 - 0.5 \cdot z$

and F(z) is a function of FSL

$F_1(z) = 1 - FSL \cdot$ *if* $FSL < 1.0$

$F_1(z) = 0$ *if* $FLS \geq 1.0$

The ranges of LPI associated to the different hazard levels are reported in Table 1.

Table 1. LPI classification hazard level.

LPI range	**Liquefaction risk**
LPI = 0	very low
0 < LPI <5	low
5 < LPI < 15	high

b) "Post-liquefaction subsidence – W" (Zhang et al., 2002),

$$w = \int_0^Z \varepsilon_v(z) \cdot dz \quad (3)$$

where $\varepsilon_v(z)$ is the volumetric deformation at depth z computed in Figure 1 as function of the safety factor (Equation 1) and of the normalized CPT resistance.

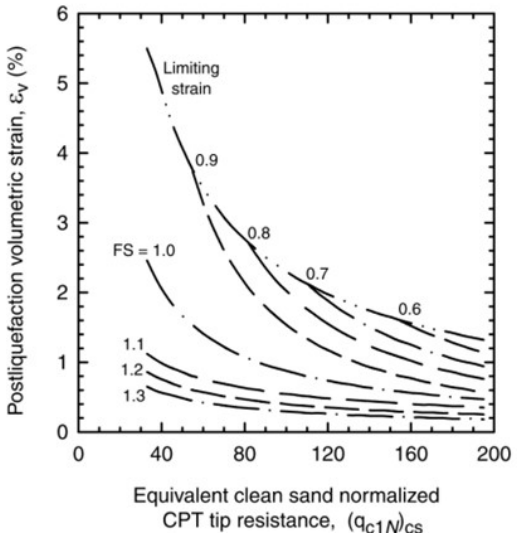

Figure 1. Post-liquefaction volumetric strain (Zhang et al., 2002).

c) "Liquefaction Severity Number - LSN" (van Ballegooy et al., 2014)

Here the indicator is integrated as follows:

$$LSN = 1000 \cdot \int_{0\,m}^{20\,m} \frac{\varepsilon_v(z)}{z} \cdot dz \quad (4)$$

where $\varepsilon_v(z)$ is the volumetric defomatiom at the depth z, computed as above.

Table 2 reports the LSN ranges associated to the effects at the ground level:

Table 2. LSN ranges and observed land effects.

LSN	**Related effect**
0-10	Little to no expression of liquefaction, minor effects
10-20	Minor expression of liquefaction, some sand boils
20-30	Moderate expression of liquefaction, with sand boils and some structural damage
30-40	Moderate to severe expression of liquefaction, settlements can cause structural damage
40-50	Major expression od liquefaction, undulations and damage to ground surface, sever total and differential settlement of structure
+50	Severe damage, extensive evidence of liquefaction at surface, severe total and differential settlements affecting structures, damage to services

2.2 Liquefaction hazard mapping

The geostatistical approach (Chiles and Delfiner, 1999) aims to represent spatially the physical quantities known only on a limited number of measurement points. Its basic principle is to interpolate information on single positions exploiting the natural structure of their spatial distribution. All distributions are in fact characterized by an inherent structure connected with the origin and the continuous development of the generating phenomenon. For instance, the stratigraphy of the subsoil is the result of depositional process and the transition from one subsoil type to the other is not random, but dictated by some physical law. The geostatistical methods study the mathematical structure of this transitions on a statistical basis and use theoretical models to simulate the variability of a certain quantity and interpolate it across known values.

One basic assumption is that the value of a variable in a single point somehow depend on the values measured at distinct locations. More precisely, values at neighboring points are more closely related than values measured at distant points. This spatial correlation constitutes the structure of the regionalized phenomenon. This structure is quantified by a variogram function γ(h), that defines the variation of a quantity z as function of the distance between the considered couple of points. The theoretical variogram (Figure 2), which describes the spatial structure of the regionalized variable, is obtained interpolating in the γ(h) plane all the points computed from the dataset with the following function.

Errore. Il segnalibro non è definito. $$\gamma(h) = \frac{1}{2N(h)} \sum_{i=1}^{N(h)} \left(z(i) - z(i+h)\right)^2 \quad (5)$$

where z is the occurrence of the studied variable, h the distance between the considered couple of points, N(h) the number of couples having distance equal to h. The spherical model has been assumed in the present study to interpolate the statistical distribution (Equation 6).

Errore. Il segnalibro non è definito. $$\gamma(h)=\begin{cases} C\left(\frac{3}{2}\frac{h}{a}-\frac{1}{2}\frac{h^3}{a^3}\right) & 0\le h\le a \\ C & h>a \end{cases} \quad (6)$$

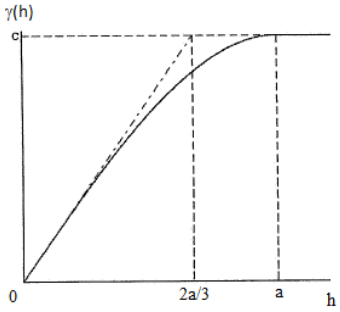

Figure 2. Spherical variogram.

In general, the difference grows with the distance h, but a limit value γ (∞) =C ("sill") is introduced as a parameter of the model. The other important parameter is *a* ("range") that represents the distance where similarity is larger. The range leads to the notion of the "area of influence" of a value. Beyond *a*, the variogram assumes a constant value equal to the sill *C*, and the variables Z(x) and Z(x+h) are not related each other (e.g. they are independent).
The interpolator used in Geostatistical analyses, called Kriging is based on the theoretical variogram. It provides punctual estimates the value of the variable in each node (x_o) of the studied space with the following linear functions of the measured values at position x_α:

$$Z^*(x_0)=\sum_{\alpha=1}^{n}\lambda_\alpha Z(x_\alpha) \quad (7)$$

The weights λ_α are evaluated considering:

- the distances between the points to be estimated and observed points;
- the geometric configuration of the observed points;
- the spatial structure of the regionalization described by the variogram γ.

The expected value of the error of estimation can be also computed as follows:

$$E\left[Z^*(x_0)-Z(x_0)\right]=m\left(\sum_{\alpha=1}^{n}\lambda_\alpha-1\right) \quad (8)$$

In the case of the punctual ordinary kriging, where the mean (m) is unknown, the variance of estimation-error $Var[Z^*(x_0)-Z(x_0)]$ needs to be minimized to adhere with the required of the absence of dual-distortion, i.e. $\sum_{\alpha=1}^{n}\lambda_\alpha=1$.
The above algorithms have been implemented to compute the spatial distributions of the liquefaction potential indicators. The calculation procedure has been implemented with the two subsequent steps:

a) homogenization of the CPT output and automated calculation of the indicators;
b) representation of the results on a Geographical Information System platform and application of geostatistical tools to map the liquefaction potential indexes.

3. DELIMITATION OF THE LIQUEFIABLE DEPOSITS

The second analysis concerns the localization of the subsoil volume prone to develop liquefaction. Such a study is fundamental when strategies are undertaken to mitigate the effects of liquefaction with ground improvement methodologies. The first step is the determination of homogeneous soil layers within the CPT profile. With this aim, statistical analyses have been developed over the years to enable a less subjective interpretation of the data. In the present study, the cone resistance q_c and sleeve friction f_s have been statistically analyzed to identify the lithological discontinuities and reconstruct the stratigraphic profiles (e.g. Lo Presti et al., 2009).

Among the statistical tests suggested in the literature, the method proposed by Wickremesinghe and Campanella (1991) is based on the introduction of the intra-class correlation coefficient. In this work, an evolution of this method has been applied based on a geostatistical approach proposed by Spacagna et al. (2015). The latter method provides a more accurate interpretation of the CPT tests that takes into account the spatial correlation of the measured values.

This test is based on the statistical test aimed to verify the equality of the means and the variance of two subset of data, according to the procedure shown in Figure 3. With regard to the parameters of CPT test (cone resistance, q_c, lateral resistance, f_s) along the vertical axis, a window W_{d0} is centered around the point d_0. The depth where the point d_0 is located has been assumed as the transition between two different lithological layers. Then, the window W_{d0} includes two subsets of data, namely Ω_1 and Ω_2, with size respectively equal to n_1 and n_2, average $\overline{Q_1}$ and $\overline{Q_2}$ and variance σ_1^2 and σ_2^2.

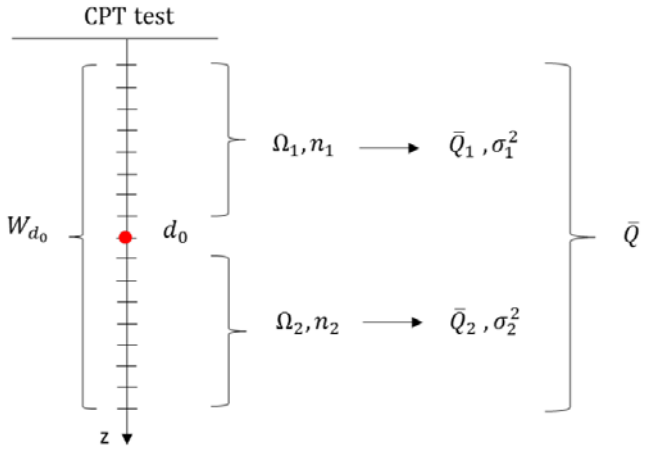

Figure 3. Definition of the two subsets of relevant parameters along the vertical axis of CPT test

The value of the T ratio is defined in the Equation (9):

$$T = \frac{\overline{Q_1} - \overline{Q_2}}{\gamma_w} \sqrt{\frac{n_1 n_2}{n_1 + n_2}} \tag{9}$$

Where

$$\gamma_w = \frac{n_1}{n_1 + n_2 - 1}\sigma_1^2 + \frac{n_2}{n_1 + n_2 - 1}\sigma_2^2 \tag{10}$$

$$\sigma_1^2 = \frac{1}{(n_1 - 1)} \sum_{i=1}^{n_1} \left(Q_i - \overline{Q_1}\right)^2 \tag{11}$$

$$\sigma_2^2 = \frac{1}{(n_2 - 1)} \sum_{i=1}^{n_2} \left(Q_i - \overline{Q_2}\right)^2 \tag{12}$$

The intra-class correlation coefficient ρ_I is calculated using Equation 13.

$$\rho_I = \frac{\gamma_b^2}{\gamma_b^2 + \gamma_w^2} \tag{13}$$

The variance between class γ_b^2 is defined by the Equation 14:

$$\gamma_b^2 = \frac{1}{n_1 + n_2 - 1} \sum_{i=1}^{n_1+n_2} \left(Q_i - \overline{Q}\right)^2 \tag{14}$$

where $\overline{Q}$ is the average of the data Q_i belonging to the window w_{d0}, with i=1,2, ..., $(n_1 + n_2)$.
To define the window W_{d0}, the geostatitcal approach proposed by Spacagna et al. (2015) suggests to calculate the one-dimensional experimental variogram of the variable, with lag equal to the minimum distance of measured point. The variable is spatially correlated if the measure points were distant not more than the "range". This parameter gives a proper definition of the amplitude of W_{d0} used for the statistical test.
The T ratio and ρ_I are calculated for each point d_0. Along the two new profiles, higher values of T ratio and ρ_I correspond to a change of behavior of the CPT parameters (qc and fs). Therefore, it is necessary to identify the critical value of the T ratio and ρ_I in order to define a potential change of layer. The statistical analysis of the value of T ratio and ρ_I, allowed to check the normality of the distribution of these parameters, by performing goodness of fit tests (Kolmogorov-Smirnov test). This test analyzes the discrepancy between observed values and the values expected under the hypothesized model.
The critical value of the parameter T and ρ_I have been calculated as follows:

$$t_c = \mu_{T\,ratio} \pm 1{,}65\, \sigma_{T\,ratio} \tag{15}$$

where $\mu_{T\,ratio}$ and $\sigma_{T\,ratio}$ are respectively mean and standard deviation of the normal distribution of the variable T.

$$\rho_{Ic} = \mu_{\rho_I} \pm 1{,}65\, \sigma_{\rho_I} \tag{16}$$

where μ_{ρ_I} and σ_{ρ_I} are respectively the mean and standard deviation of the normal distribution of the variable ρ_I.

4. THE CASE STUDY

In May and June 2012, a wide portion of the territory of the Po Valley (in Emilia Romagna Region, Italy) was affected by a significant seismic activity of over 2500 events, of which 7 with magnitude greater than 5 (Figure 4.a). The liquefaction affected the entire fluvial plain of the Ferrara area, especially in the municipalities of Sant'Agostino and Mirabello, along the North East - South West alignment of the old riverbed of the Reno River (Figure 4.b).
One of the most affected area is the district of San Carlo (in the Municipality of Sant'Agostino), which rests on a plain formed by the Reno River, subsequently (18th century) diverted to the Southeast direction to avoid recurrent overflowing of the plain of Ferrara.
The Emilia Romagna Region provides a database of geophysical tests performed throughout the territory. For Sant'Agostino, 330 CPT tests have been collected, 75 of which are located in the San Carlo district (Figure 5).
The available database of CPT tests includes both mechanical (CPTm) and electric (CPTe) tests. It is worth reminding that the methods adopted to compute FSL (e.g. Boulanger Idriss 2014) is based on

CPTe test, and so its application to CPTm tests could lead to erroneous predictions and wrong estimates of the liquefaction potential. The main differences between CPTe and CPTm consist of:

- the geometry of the tip, the application of stab strength and the acquisition the information;
- the size of the investigated soil volume (CPTm measures are spaced 20 cm, while CPTe 2 cm);
- the possible uncontrolled inclination from the initial vertical position for the CPTm.

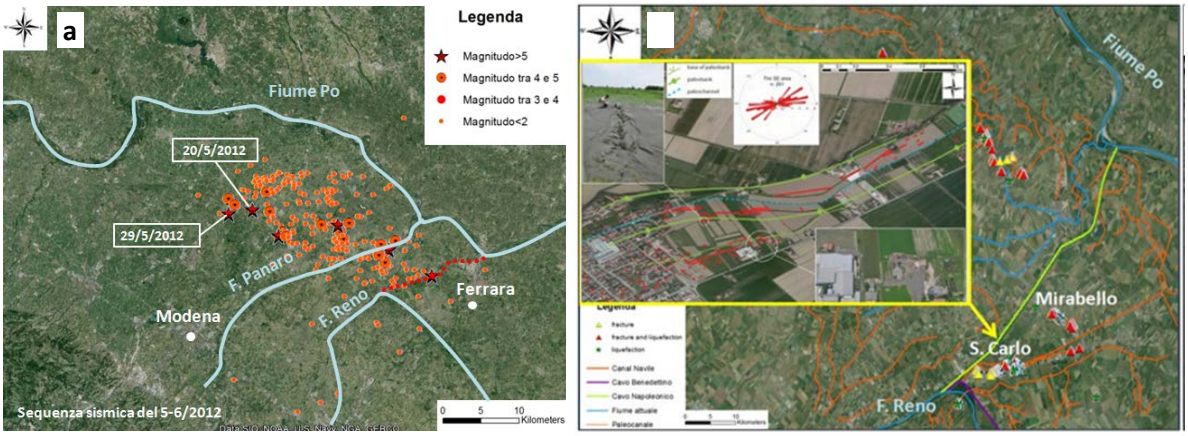

Figure 4. a) seismic sequence characterized by two major earthquakes, the first occurred on May 20, 2012 with magnitude Mw = 5.9 and hypocentral depth of 6.3 km; the second, of 29 May, with Mw = 5.8 and hypocentral depth of 10.2 km. b) Localization of the old fluvial plain of the Reno River, and San Carlo district.

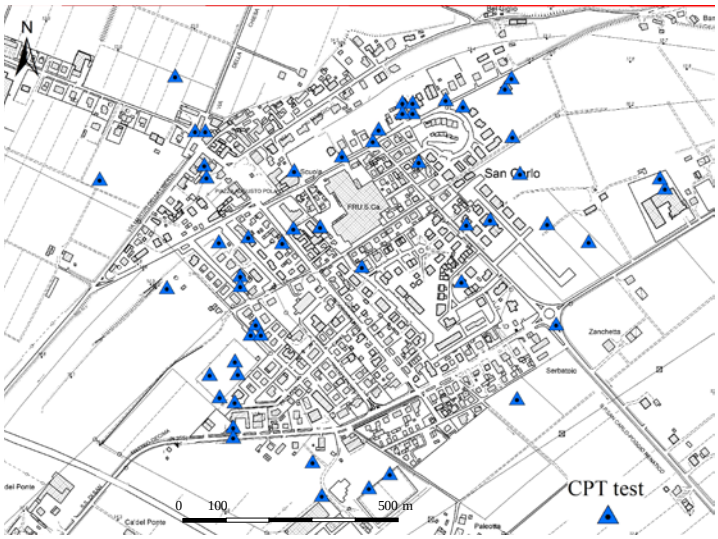

Figure 5. CPT tests available in San Carlo district

Based on data from 44 couples of mechanical and electrical CPTs performed 1-3 m far each other, Madiai et al. (2016) evaluated the Liquefaction Potential Index (LPI) for the 2012 Emilia Romagna earthquake, in order to propose a procedure to calibrate the results obtained from CPT and use them for Liquefaction Risk evaluation. The corrections for the normalized tip resistance ($q_{c1n,cs}$) and for the material index I_c are reported in Figure 6.

The above corrections have been applied to homogenize the CPT dataset and, given the considerable amount of data that need to be processed, the calculation of the indexes has been automatized with a script implemented with R software (www.r-project.org).

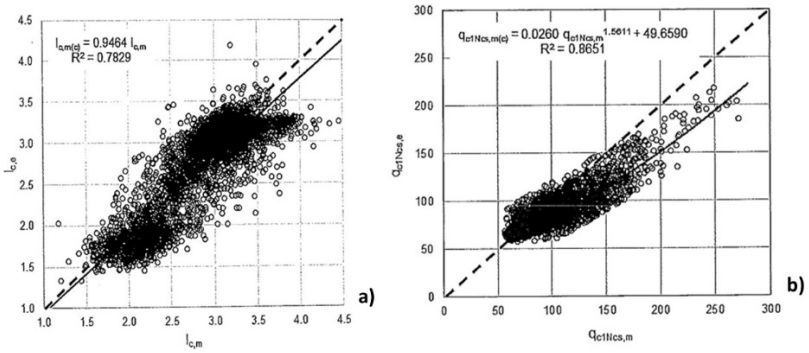

Figure 6. Regression model for the correction of I_c (a) and $q_{c1n,cs}$ data obtained with mechanical CPTm tests (from Madiai et al. 2016).

The values of LPI, W and LSN have then been computed for each available CPT with reference to the earthquake of May 20, 2012 (Mw=5.9). The results have then been collected in a GIS platform (http://qgis.osgeo.org) and interpolated with the geostatistical methods described above. Together with the estimate of the indexes for location not covered by investigations, the adopted methodology enables to compute the estimation error, fundamental for the assessment of reliability.

The spatial distribution of LPI, LSN and W are reported in respectively Figure 7, 8 and 9. In particular, the Figures 7.a, 8.a and 9.a show the distribution of the liquefaction potential indicators together with the position of ground failures and damaged buildings noticed after the earthquake, while the Figures 7.b, 8.b and 9.b report the maps with the estimation error and the position of the CPT tests.

At first glance there is an overall similarity among the different plots, obviously considering each variable with its proper scale. However, a more detailed insight reveals significant differences in the spatial distributions of the considered variables and in the comparison with the observed damages. The LPI classification (see Table 1) is not particularly detailed and thus only two zones can be distinguished on the map of Figure 7.a, the green and yellow indicative of respectively low and high liquefaction potential. The overlapping with damage is fairly good, although there is some inconsistency in the central zone of the village, where large recorded damages of buildings and ground fall in the green zone. The plot of post liquefaction settlements (Figure 8.a) shows a red zone in the north-west part of the map, indicative of a critical subsoil layer, and a diffused light-yellow colour all over the village, representative of lower but still significant settlements. The distribution of LSN (Figure 9.a) shows comparatively less marked differences among the distinct zones of the map, possibly because the depth of the liquefiable layers is different from place to place (see Equation 4). In all plots there is relatively good overlapping of the liquefaction potential indicators with the damages observed apart from the central area of the village where noticed failures fall in zones characterized by low values of the indicators. However, it must be noticed that in this area, the estimate error for all the computed variables is particularly relevant mostly because of the limited number of CPT here available. This observation highlights the importance of associating the estimate of the damage indicator with the error of the estimate, that is possible with the adopted geostatistical approach, to quantify the reliability of prediction. The maps of the estimation error are also particularly important because they may assist the planning of new investigations. Additional CPT must be performed with a higher priority where the error is maximum.

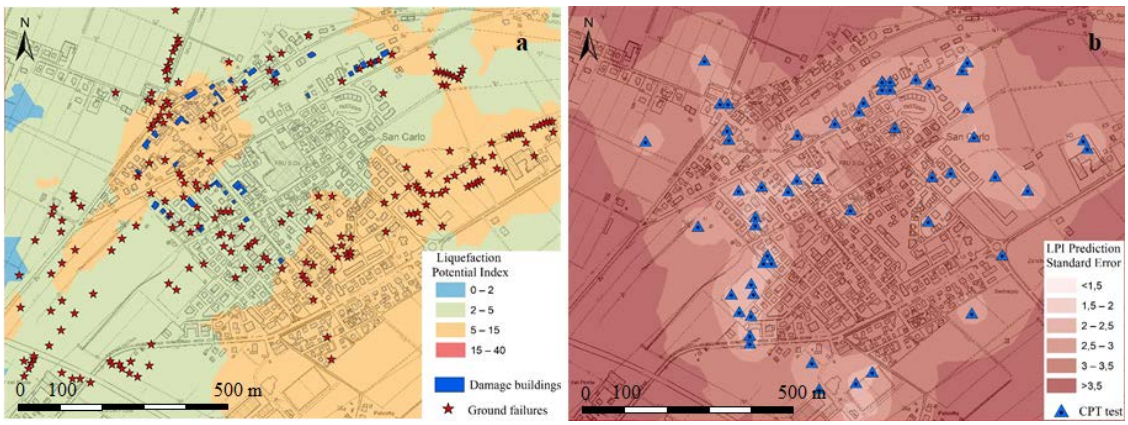

(a) (b)

Figure 7. Liquefaction Potential Index LPI (a. map and observed damages; b. estimate error and position of CPT tests).

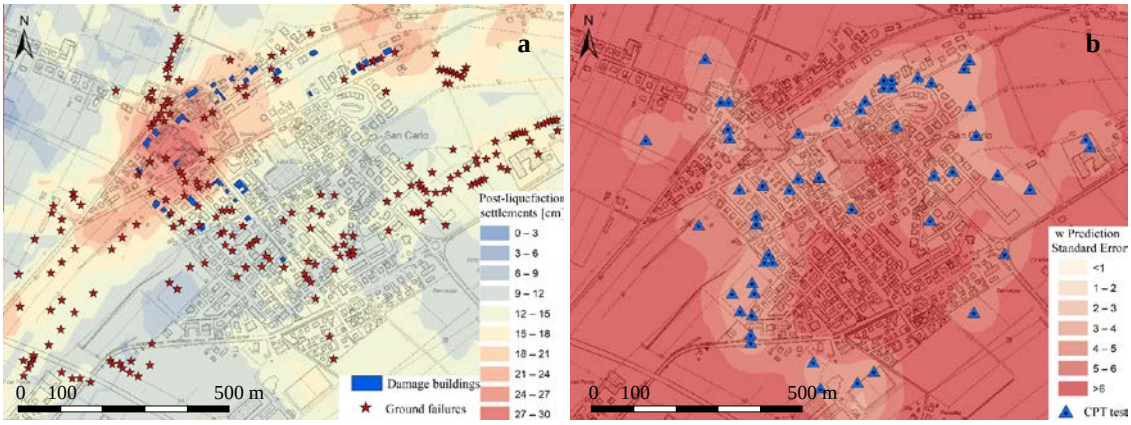

(a) (b)

Figure 8. Post liquefaction settlements (a. map and observed damages; b. estimate error and position of CPT tests).

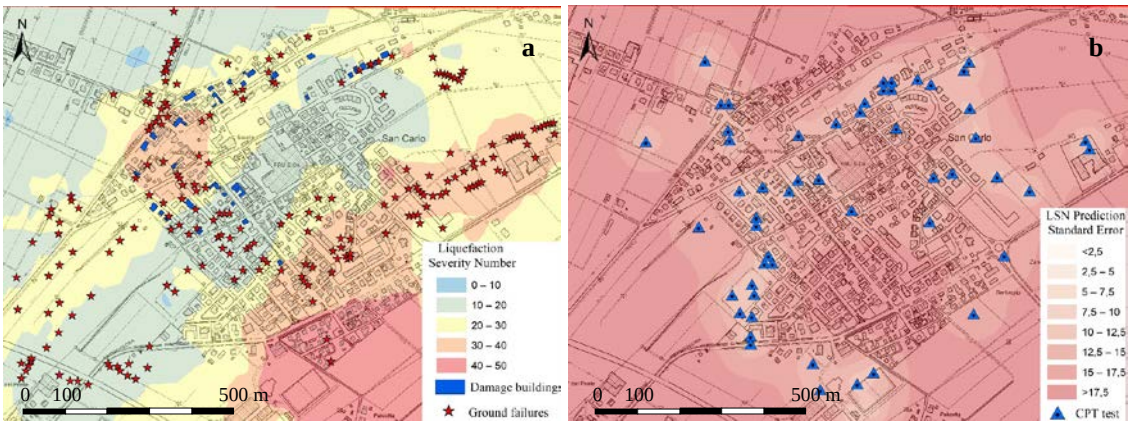

(a) (b)

Figure 9. Liquefaction Severity Number LSN (a. map and observed damages; b. estimate error and position of CPT tests).

The above maps show also, with just few exceptions, that the areas where the liquefaction potential is higher recursively occupy the same zone of the territory, for instance the strip running from west to north-east of the village. This occurrence suggests identifying the subsoil portions more exposed to

liquefaction and to delimit it. With this aim, the CPT tests are processed by applying the method described in the previous section 3 and identifying the top and bottom depth, and thus the thickness of the liquefiable layer. Finally, a spatial analysis has been accomplished interpolating the top and bottom surfaces and build a three-dimensional representation the liquefiable deposit (Figure 10).
It is worth comparing the thickness of the liquefiable deposit with the geomorphological structure of the San Carlo area (Figure 10.b) to see that the largest thickness of the potentially liquefiable soil corresponds to the position of the bed and levees of the paleo-channel of the Reno River, running from the east to the north-west of the village.

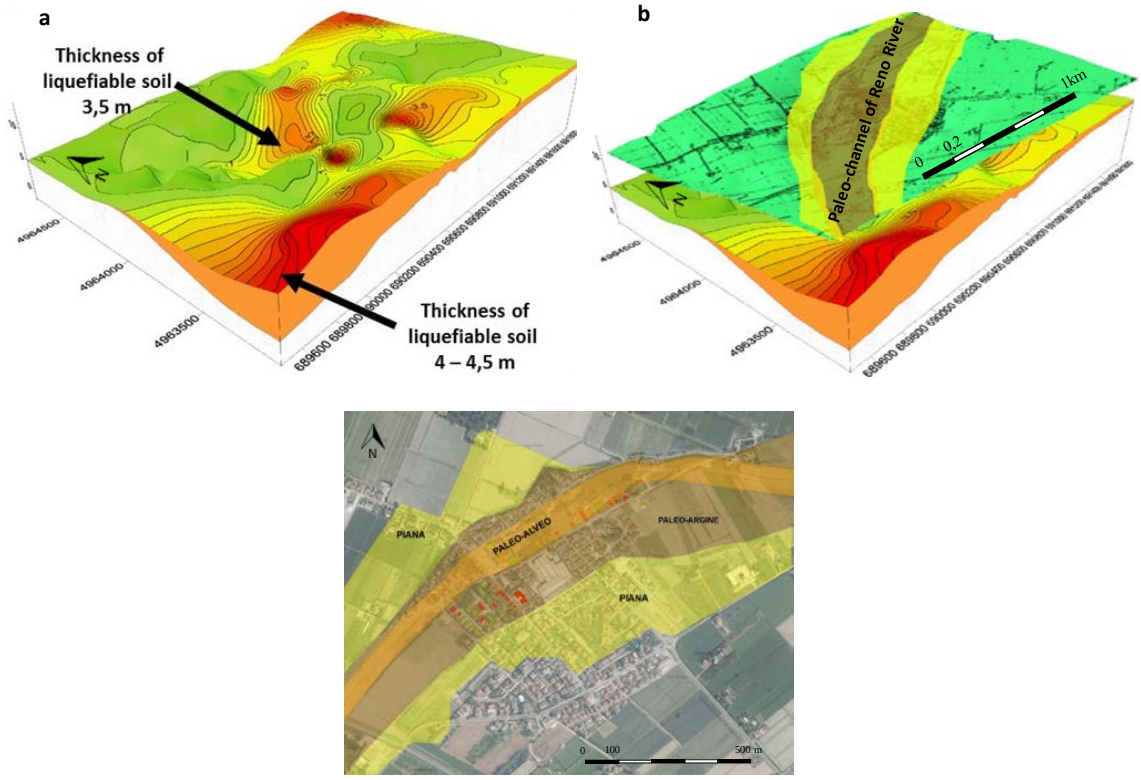

c)

Figure 10. Three-dimensional reconstruction of liquefiable deposit (a and b) overlap with the paleo channel (b and c) in the area of San Carlo district,

5. CONCLUSIONS

The paper describes a methodology to define the spatial distribution of the liquefaction hazard over large territories based on the geostatistical analysis of CPT test results. The methodology has been applied for validation to the case study of San Carlo (fraction of the municipality of Sant'Agostino-Italy), located near the epicenter of the 2012 Emilia Romagna earthquake (Mw = 6.15). Here seventy-five CPT tests have been processed with an automated procedure, homogenizing the mechanical and electrical CPT tests with an empirical formula found by Madiai et al. (2016). The validation test has demonstrated that the proposed methodology is particularly effective for the mapping of the liquefaction potential, consistently with the phenomena observed after the 2012 earthquake. Differences connected with the inherent definition of each variable exist between the maps drawn for the "Liquefaction Potential Index" (Iwasaki et al., 1978), the post-liquefaction settlement (Zhang et al., 2002) and the "Liquefaction Severity Number" (van Ballegooy et al., 2014), all computed based on the CPT profiles. The kriging used to interpolate the values of the indicator computed on each vertical over the studied area allows also to compute the error associated with the estimates. This information is particularly useful because it is possible to associate the reliability to the estimate and to fill the gap of information planning future investigations.
For instance, with regard to the present case study, the lack of CPT tests in the central area of the San

Carlo village explains the inconsistency between the estimated indicators and the observed ground and building damages.
Finally, the geostatistical analysis of the CPT profile has enabled to identify top and bottom depth of the liquefiable layer and to explain its origin connected with the paleo-channel of Reno river flowing in the north-west portion of the village.

6. ACKNOWLEDGMENTS

The authors wish to acknowledge the contribution by the EU funded project LIQUEFACT "Assessment and mitigation of liquefaction potential across Europe: a holistic approach to protect structures/infrastructures for improved resilience to earthquake-induced liquefaction disasters", project ID 700748 funded under the H2020-DRS-2015.

7. REFERENCES

Boulanger R W, Idriss I M (2014). CPT and SPT based liquefaction triggering procedures. *Department of Civil and Environmental engineering, University of California at Davis*.

Chiles, J., & Delfiner, P. (1999). Geostatistics: modeling spatial uncertainty. *John Wiley & Sons, New York*, 720p

CTMS, Commissione Tecnica per la Microzonazione Sismica, 2017, Microzonazione sismica - Linee guida per la gestione del territorio in aree interessate da liquefazione (LQ), Dipartimento della Protezione Civile e Conferenza delle Regioni e delle Province Autonome, 2008, Indirizzi e Crtieri per la Microzonazione Sismica, 150 pp.

Iwasaki T., Tatsuoka F., Tokida K., Yasuda S. (1978). A Practical method for assessing soil liquefaction potential based on case studies at various sites in Japan. *2nd International conference on Microzonation*. 1978. pp. 885-896.

Lo Presti, D., Meisina, C., Squeglia, N. (2009). Applicazione delle prove penetrometriche statiche nella ricostruzione del profilo stratigrafico. *Rivisita Italia di Geotecnica*.

Liu C.-N. and Chen C.-H. (2006). Mapping Liquefaction Potential Considering Spatial Correlations of CPT Measurements. *J. Geotech. Geoenviron. Eng.* 2006.132:1178-1187.

Madiai C., Vannucchi G., Baglione M., Martelli L., Veronese T. (2016) Utilizzo di prove penetrometriche statiche a punta meccanica per la stima del potenziale di liquefazione, Rivista Italiana di Geotecnica 3/16, pp.14-24.

Pokhrel R. M., Kuwano J., Tachibana S. (2013). A kriging method of interpolation used to map liquefaction potential over alluvial ground A kriging method of interpolation used to map liquefaction potential over alluvial ground. *Engineering Geology* 152 (2013) 26–37

Robertson, P., Cabal, K. (2010). Guide to Cone Penetration Testing for Geotechnical Engineering. *Gregg Drilling and Testing, Inc*., 138 p.

Seed H.B., Idriss I.M. (1971). Simplified procedure for evaluating soil liquefaction potential. *Journal of the Soil Mechanics and Foundations Division, ASCE*, 97(SM9): 1249–1273.

Spacagna R. L., de Fouquet C., Russo G. (2015) Interpretation of CPTU tests with statistical and geostatistical methods. *Geotechnical Safety and Risk V. T. Schweckendiek et al. (Eds.)*. pp 892-897

van Ballegooy S., Malan P., Lacrosse V., Jacka M.E., Cubrinovski M., Bray J.D., O'Rourke T.D., Crawford S.A., Cowan H. (2014). Assessment of Liquefaction-Induced Land Damage for Residential Christchurch. *Earthquake Spectra, Volume 30, No. 1*, pages 31–55, February 2014.

Wickremesinghe , D., Campanella, R. (1991). Statistical Methods of Soil Layer Boundary Location Using the Cone Penetration Test, *Proc., 6 th Int. Conf. on application of Statistics and Probability in Civil Engineering*, CERRA-ICASP6, 636-644.

Zhang G., Robertson P.K., Brachman R.W.I. (2002). Estimating liquefaction-induced ground settlements from CPT for level ground. *Canadian Geotechnical Journal*, 39, 1168–80.